Materials and Design 189 (2020) 108529

Contents lists available at ScienceDirect

Materials and Design

journal homepage: www.elsevier.com/locate/matdes

The effect of oxidising thermal exposures on the fatigue properties of a polycrystalline powder metallurgy nickel-based superalloy

D.T.S. Lewis [a,*], R.G. Ding [b], M.T. Whittaker [a], P.M. Mignanelli [c], M.C. Hardy [c]

[a] Institute of Structural Materials, College of Engineering, Swansea University, Swansea, SA1 8EN, United Kingdom
[b] School of Metallurgy and Materials, Birmingham University, Birmingham B15 2SE,
[c] Rolls-Royce plc., P.O. Box 31, Derby, DE24 8BJ, United Kingdom

HIGHLIGHTS

- 1 μm and 3 μm thermal exposures caused decreased fatigue life.
- 5 μm thermal exposure caused life improvement compared to 3 μm.
- Tertiary γ' growth, γ' depletion, recrystallised grains and decreased surface roughness may cause the improved life.
- Oxidation of notched fatigue specimens has reduced effect in reducing the fatigue life compared to plain specimens.

GRAPHICAL ABSTRACT

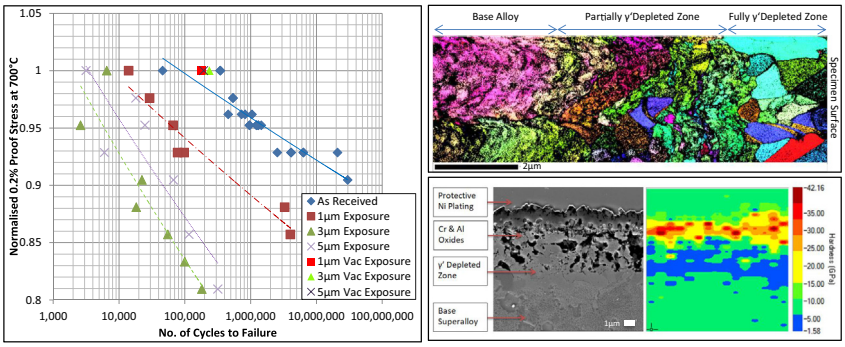

ARTICLE INFO

Article history:
Received 11 November 2019
Received in revised form 6 January 2020
Accepted 27 January 2020
Available online 28 January 2020

Keywords:
Ni-based superalloys
Fatigue behaviour
Micro-/nanoindentation
Profilometry
Transmission electron microscopy (TEM)

ABSTRACT

A number of thermal exposures were undertaken to determine the effect oxidation has on the fatigue lives of the nickel-based superalloy RR1000. The thermal exposures initially caused a considerable reduction in the fatigue lives with increasing oxidation. However, the longest exposure time resulted in an S-N curve that lay between the shortest and mid length exposure. A range of analyses were undertaken to determine the presence of any mechanisms that could have caused this unexpected life increase; vacuum thermal exposures, small punch tensile, nanoindentation, microscopy and transmission Kikuchi diffraction. It was found that few of the mechanisms investigated were likely to have an effect on the change in life with the exceptions being; reduction in dislocation movement and crack deflection as a result of a recrystallised zone at the surface, variation in hardness of different regions due to a γ′ depleted plastic zone and a hard ceramic oxide, and reduced initiations due to the presence of a 'healing' chromium oxide scale. Notch fatigue tests were performed to determine the importance of the findings to components in service and it was found that the notch acted as the cause of crack initiation, effectively mitigating against the effects of the oxidation damage.

1. Introduction

Environmental degradation is a key element which affects the performance of mechanical components in an aero-engine, particularly those that operate in the high temperature oxidising environments of

* Corresponding author.
E-mail address: d.t.s.lewis@swansea.ac.uk (D.T.S. Lewis).

https://doi.org/10.1016/j.matdes.2020.108529

the high pressure turbine (HPT) section. Furthermore, oxidation is becoming increasingly important as the operating temperatures within the aero-engine are increasing in order to improve fuel efficiency, reduce the production of harmful emissions, and subsequently pushing the materials towards the edge of their operating window.

Nickel-based superalloys have been optimised to operate in these harsh, high temperature and high pressure environments, through both compositional and microstructural optimisation. It has previously been found that when these nickel-based superalloys oxidise, a chromium oxide scale is formed at the surface creating a thin layer with rutile (titanium oxide) nodules on the outer surface, along with subsurface aluminium oxide in the form of intergranular 'fingers' and intragranular 'islands' [1–7]. Deeper into the substrate material a weaker γ′ (nominally Ni_3(Al, Ti)) depleted zone is present due to the migration of elements to form the aluminium and titanium oxides [2–4,7]. The final damage that will occur into the specimen is deeper grain boundary carbide depletion, which is the result of chromium migration from the grain boundary, MC and $M_{23}C_6$ carbides, to form the surface oxide scale [8–10].

Previous studies have found that cyclic loading commonly leads to a decrease in fatigue life in the nickel superalloys LSHR and ME3 [7,11], and fatigue loading was found to increase the rate of oxidation in coarse grain RR1000 and an unnamed powder nickel based superalloy [6,12,13]. It is the aim of this study to understand how oxidation affects the fatigue performance of the alloy. A range of thermal exposures have been chosen to provide a wide range of outcomes. It has previously been found that oxidation has a large effect on the fatigue lives of nickel-based superalloys, most notably during the crack initiation stage [3,6,12,14,15]. Three different exposures were defined and a range of load controlled fatigue tests were performed to investigate how they affect fatigue life.

Given advances in technologies and the wider availability of more complex analysis methods, it is possible to investigate the comprehensively studied fatigue properties of these materials in novel ways. The current paper seeks to undertake this through higher magnification imaging using field emission gun scanning electron microscopy (FEG SEM) and scanning transmission electron microscopy (STEM), nanoindentation and testing approaches such as Small Punch Tensile (SPT) allowing for a broad ranging study.

2. Experimental method

The material considered throughout the investigation is fine grain RR1000, the composition of which is shown in Table 1.

It is a polycrystalline powder metallurgy nickel-based superalloy with a typical grain size of 4–11 μm [16], which includes a tri-modal γ′ phase with a volume fraction of 45%. The alloy is strengthened through the precipitation the secondary and tertiary γ′ phases (Ni_3(Al, Ti, Ta) from the FCC γ matrix; secondary γ′ is between 50 nm and 500 nm in diameter and tertiary γ′ is under 50 nm, with an average of 15 nm in diameter. All fatigue specimens were shot peened under representative in service conditions, i.e. 110H, 6–8A and 200% (hardness of the shot, peening intensity and shot coverage).

A series of fatigue tests were conducted in a laboratory environment on shot peened cylindrical bar plain fatigue specimens that had undergone a range of thermal exposures to produce specific oxide depths of 1 μm, 3 μm and 5 μm according to the following thermal exposures: 1 μm exposure for 72 h at 700 °C, 3 μm exposure for 211 h at 740 °C and 5 μm exposure for 310 h at 762 °C, were performed in a standard desktop furnace. These different temperatures were used in order to produce oxide depths within reasonable timeframes. Load controlled fatigue testing was then performed at 700 °C at a range of stresses to generate S-N curves and data from these tests compared to existing data for as received specimens to provide a base line.

Following on from these tests a series of thermal exposures were performed on a number of plain fatigue specimens in a vacuum furnace, according to the 1 μm exposure, 3 μm exposure and 5 μm exposure thermal profiles in order to discount any effects of the heat treatments on material evolution in the substrate. Fatigue tests for each thermal exposure condition were then performed according to the same test standard as the initial investigations but with all tests performed at 1050 MPa.

Subsequently, the testing method of small punch tensile (SPT) was utilised to determine if there was any change in mechanical properties as a result of microstructural evolution. Testing was performed on 8 mm diameter × 500 μm thick disks taken from 4 rods of the alloy, three of which had undergone the range of thermal exposures. Tests were performed in accordance with the European Code of Practice for Small Punch [17]. The advantage of SPT for this instance is the fact that all the oxidised surfaces of the disc would be in the clamped area of the test setup, and therefore, would in no way influence the output data.

The nanoindentation method of accelerated property mapping (XPM) using a Berkovich indenter was employed in this study to analyse the changes in the hardness and ductility of the oxide products and also the subsurface regions affected by the oxidation process. For correlation purposes with the nanoindentation, ambient temperature micro hardness analysis using the Vickers Hardness method was also performed applying 1 kgf for a dwell of 10 s.

A final set of fatigue tests were then performed on notched fatigue specimens, which were flat double notched specimens at 2 different stress concentration factors, 1.55 Kt and 2.29 Kt. A number of the specimens were tested in the as received condition, and these were compared to specimens that were exposed according to the 3 μm exposure. LCF tests were undertaken following the same test standard as the plain fatigue specimens and data from these tests was compared to existing data for similar notch geometries.

Following fatigue testing, micrographs were produced using scanning electron microscopy (SEM) and transmission electron microscopy (TEM) to investigate any features of note. Also used for the analysis was an Alicona Infinite Focus profilometer, in order to establish the surface roughness values (S_a) of the specimens using the standard ISO 25178. S_a is an extension of R_a, the more commonly used linear surface roughness measurement, using areal measurements. This is seen as being a more accurate measure of surface roughness as it works on 3D rather than 2D information and is less likely to miss or conversely be influenced by anomalies within an investigated surface.

Table 1
RR1000 composition in weight percentage.

Ni	Co	Cr	Mo	Al	Ta	Ti	C	B	Zr	Hf
Bal	18.5	15	5	3	2	3.6	0.03	0.02	0.06	0.5

3. Results and discussion

Specimens were pre-exposed to the different damage depths as can be seen in Fig. 1, with the typical chemical composition of the oxidised region shown in Fig. 2.

Cyclic endurance lives of the specimens pre-exposed in the laboratory environment were compared to as received fatigue data shown in Fig. 3. It was observed that overall, the thermal exposures reduced the fatigue lives compared to that of the as received specimens, which was as expected [6,13] and the life initially reduced for the 1 μm Exposure specimens by over 90%, with a further drop to the 3 μm Exposure specimens. However, it is shown that the 5 μm Exposure specimens outperformed the 3 μm exposure specimens, providing lives between those of the 1 μm Exposure and the 3 μm Exposure specimens. It would ordinarily be expected that the oxidation damage would lead to a decrease in the number of cycles to crack initiation, as is shown to be the case from the 1 μm exposure compared to the 3 μm exposure and 5 μm exposure heat treatments. Following on from this,

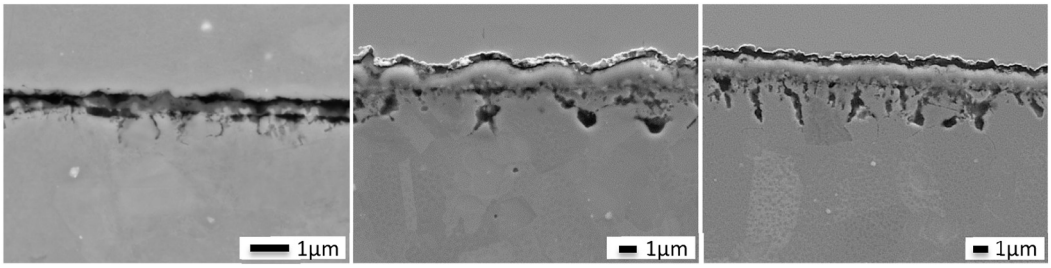

Fig. 1. BSE micrographs showing oxide accumulation (left) 1 µm exposure (center) 3 µm exposure (right) 5 µm exposure.

investigations were undertaken based on the premise that the life improvement was a result of a secondary, complementary mechanism occurring during the crack propagation or initiation stages. A number of potential causes have been investigated to determine the source of the unexpected result.

In order to determine the contribution to the fatigue life of initiation and propagation, and therefore where the focus of the investigation should be, an effective initial flaw size (EIFS) numerical analysis was performed, utilising existing fatigue crack propagation data and initial flaw sizes equal to the oxide damage depths equal to the combined chromium oxide and aluminium oxide as can be seen in Fig. 1 for each damage level. The equation used for the analysis is shown in Eq. (1).

$$N_p = \int_{a_0}^{a_f} \frac{da}{C\,\Delta K^m} = \frac{1}{C\left(Y\,\sigma\,\sqrt{\pi}\right)^m}\left[\frac{a_f^{m\prime} - a_0^{m\prime}}{m\prime}\right] \tag{1}$$

The result of the analysis can be seen in Table 2.

As can be seen, the predicted contribution of the initiation stage to the overall life accounts for the majority of the fatigue cycles. This suggests that the mechanism resulting in life increase for the 5 µm exposure specimens will most likely occur during initiation. However, it can be seen that the percentage predicted propagation life for all damage stages increases for the longer thermal exposures. However, given that these findings indicate propagation to be a relatively small fraction of the total life, it is suggested that the effect of oxidation on initiation plays the more dominant role.

SPT tests were performed on specimens that had undergone the thermal exposures to determine if there were any changes to the bulk mechanical properties of the material, whilst removing the effects of the surface from the tested region. SPT was also ideal for this investigation, as it is a useful material properties ranking tool, and only small amounts of material are required to produce specimens. Four cylindrical rods were electrical discharge machined (EDM'd) from a block of the alloy, three of which were heat treated according to the thermal exposures with the final rod left in an AR condition. The small punch specimens were then cut from the rods. It can be seen that there is some variation in the mechanical properties of the alloy under SPT testing as shown by Fig. 4. However, the tests AR1 and AR2 represent the bounds in scatter from a range of SPT tests on the same batch of material. In these extreme cases variation may be due to a compliance issue in the test at low loads or indenter wear, but encouragingly similar gradients of the curves as the load increases and near identical UTS are found.

To assess the microstructure, an investigation into the evolution of the small tertiary gamma prime (γ′) precipitates was then completed. As mentioned previously, the alloy contains a high percentage of the γ′ phase, and secondary and tertiary γ′ act to impede the movement of dislocations and retard fatigue crack growth, improving both the initiation and propagation resistance of an alloy. It has been shown that at elevated temperatures the small tertiary γ′ within the gamma matrix will coarsen or diffuse into the matrix, and upon cooling reprecipitate as a very fine tertiary γ′ [18,19]; it has long been known that precipitate size has an effect on the fatigue crack growth rates of a material [20,21]. Two methods were employed to investigate this hypothesis; fatigue tests following vacuum furnace exposures and tertiary γ′ size measurement predictions from a Rolls-Royce plc. model. The values were calculated using a tertiary γ′ size predictive model based on the Ostwald ripening process. The model is populated with a large database of tertiary γ′ sizes at a range of times and temperature measured from TEM micrographs, an example of which can be seen in Fig. 5.

In order to assess the role of tertiary γ′ on fatigue life, tests were performed following thermal exposure using a vacuum furnace according to the prior thermal exposure regimes. It was believed that by using a vacuum furnace, it would be possible to produce the microstructural changes within the bulk of the specimen whilst minimising the formation of the oxides, therefore isolating the effects of microstructural changes from the oxide damage accumulation.

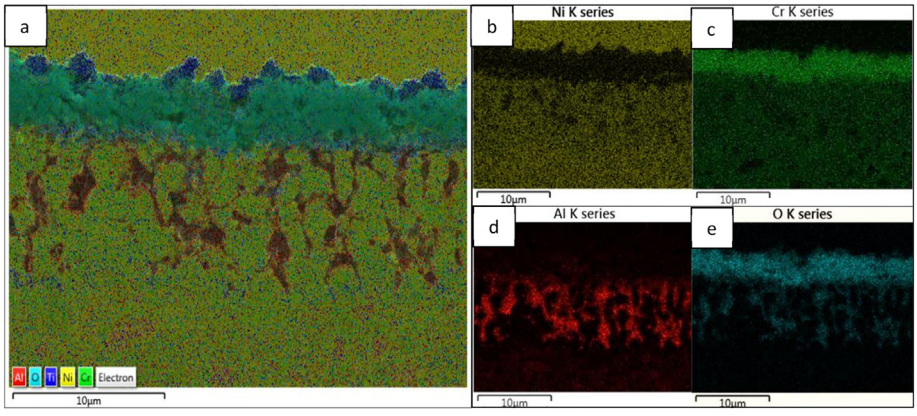

Fig. 2. EDS analysis of the oxide formation of the RR1000 following long thermal exposure (a) composite element map (b) nickel map (c) chromium map (d) aluminium map (e) oxygen map.

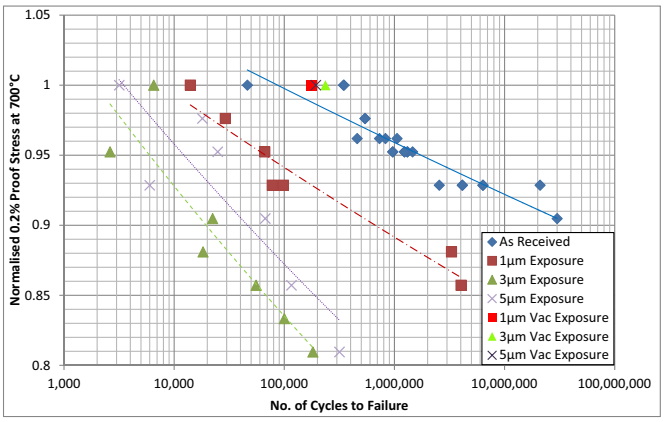

Fig. 3. Fatigue lives of specimens with increasing exposures. Decreases in fatigue life are evident in 1 µm exposure and 3 µm exposure specimens, but then lives increase from 3 µm exposure to the 5 µm exposure specimens.

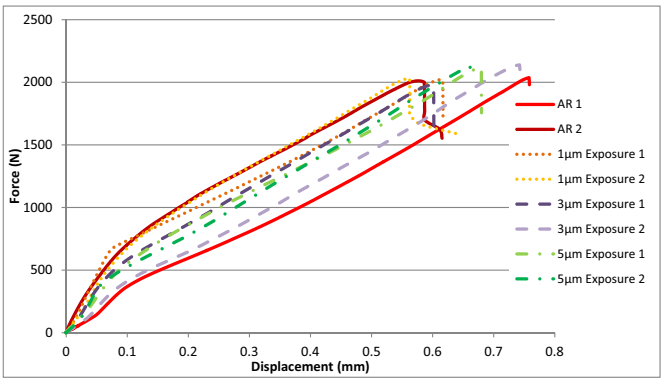

Fig. 4. Small punch tensile curves for the thermal exposure conditions and as received material.

Had there been any discernible change in the morphology of the tertiary γ′ it would be expected that the fatigue lives of the vacuum furnace exposed specimens should have longer lives than the as received specimens, and that the specimens that underwent longer thermal exposures i.e. vacuum 5 µm exposure, should have the longest lives. It was found following testing that the fatigue lives of the vacuum thermal exposure specimens were statistically indistinguishable from the initial as received specimen tests as is shown by the vacuum test values presented in Fig. 3. However, this does not address the potential that there is an unknown interaction between the coarsened or very fine tertiary γ′ and the oxide layers, meaning that the results from this line of testing are inconclusive.

To address this ambiguous finding, the Rolls Royce plc. model described above was utilised. It was found that over the heat treatments the average size went from 15 nm in the as received, to 16 nm at 1 µm exposure, 30 nm at 3 µm exposure and 44 nm for the 5 µm exposure. These changes in the tertiary γ′ size are likely to have affected the creep response the alloy, potentially affecting the fatigue life of the specimens [22,23]. Furthermore, in the case of these load control tests, conducted at stresses near to the yield point of the material, it is also possible that microstructural changes may have altered the yield stress of the material, resulting in reduced plastic strain on loading, and hence increasing fatigue life.

Further investigation were undertaken as a result of the work by Elber [24,25], which suggests that an increase in the plasticity of a material, can lead to a decrease in the rate of fatigue crack growth due to the mechanism of plasticity-induced crack closure [26]. It is understood that the γ′ depleted zone of the alloy after oxidation will have increased ductility, leading to an increase in the plasticity of the region and that this would result in an increase in the effect of plasticity-induced crack closure and therefore an increase in fatigue life. Plasticity induced crack closure may produce a reduction in the effective stress intensity range during crack growth, hence lowering crack growth rate and increasing fatigue life. However, as this is a crack propagation mechanism, this may not have a significant contribution on the overall fatigue life, based on the EIFS calculations. In order to investigate the existence of this plastic zone, XPM was undertaken in the oxidation region, the benefits of which were explained by Hintsala et al. [27].

It is difficult to assign a specific mechanism which results in the increase in fatigue life of the 5 µm exposure specimens, compared with 3 µm exposures. However, the interaction between the alumina fingers and the γ′ depleted zone may play a significant role. As is apparent in Fig. 6, there is a dramatic change in the hardness values between the ceramic oxides at the surface and the γ′ depleted zone with the base material hardness values sitting between these two extremes. The γ′ depleted zone was found to be deeper for longer thermal exposures. It is therefore possible that the reduced hardness of this γ′ depleted zone acts to reduce the effectiveness of the crack initiation mechanism from the alumina fingers, hence increasing the fatigue life.

In order to provide meaningful data to the engineering community at large it is important to relate the results from the XPM to a more common method. It is possible to approximate the H_v values from the XPM output using Eq. (2).

$$Hardness_{Vickers} \times 0.009807 \approx Hardness\ (GPa) \quad (2)$$

The data from the hardness tests is shown in Table 3 and the nano-indentation values are taken from the colour contour brackets on the XPM legend. The formula output represents the values calculated from Eq. (1) and microhardness tests which were performed on the areas that were able to be tested using the microhardness tester in order to validate the equation. As can be seen by the comparison between the

Table 2
Comparison of actual fatigue lives and predicted lives based on Paris law propagation prediction.

Thermal exposure	Actual life (cycles)	Predicted propagation life (cycles)	Predicted %propagation life of total life
1 µm Exposure	14,023	1266	9
3 µm Exposure	6524	774	12
5 µm Exposure	3170	622	20

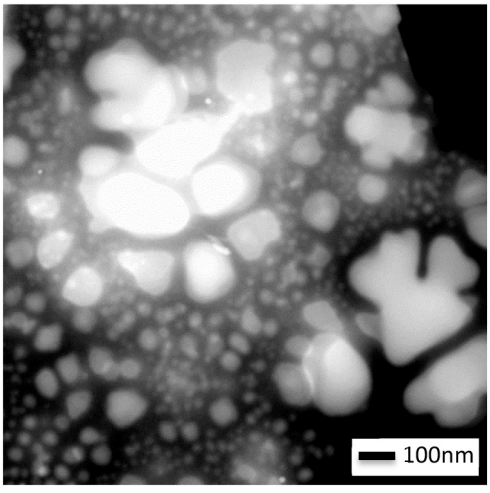

Fig. 5. High-angle annular dark-field scanning transmission electron microscopy (*HAADF-STEM*) micrograph of secondary and tertiary γ′ in an AR specimen.

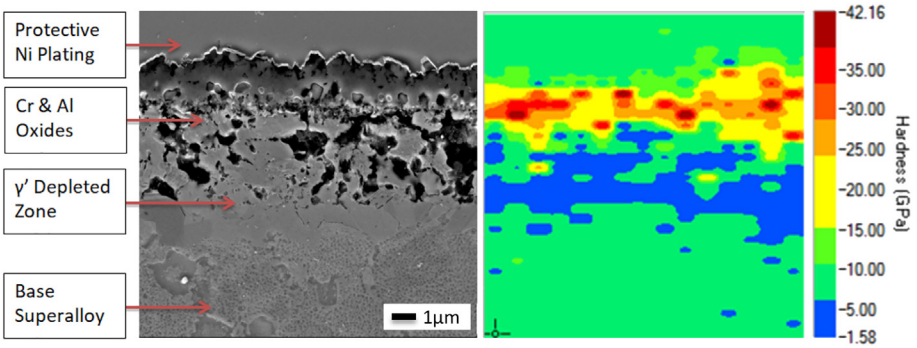

Fig. 6. SEM micrograph of the oxidised region (left) and corresponding XPM map (right) of a 5 µm exposure specimen.

Table 3
Table comparing nanohardness, microhardness and calculated values.

Location	Nanoindentation (GPa)	Eq. (1) output (H_v)	Micro hardness (H_v)
Oxides	15–42	1529–4282	1652–3508
γ′ depleted zone	1–5	102–509	–
Base alloy	5–10	509–1019	483

Eq. (1) output and the microhardness values, there is a reasonable correlation, although it should not be relied upon too heavily.

Another area of interest is the presence of a very fine grain recrystallised (Rx) region below the surface oxide scale [28,29]. It has been found that heat treatments following a plastic deformation process during manufacturing such as shot peening, can lead to this recrystallisation [30,31] in certain materials. This can result in beneficial effects for both the initiation and propagation stages. Firstly, the smaller grains would act to impede dislocation movement, reducing the chance of dislocation pileup at areas likely to lead to crack initiation of the oxidised specimen i.e. component surface. Secondly, the fatigue improvement effects on crack propagation stage would be the fatigue crack deflection mechanism as explained by Suresh [32,33], which would occur in this Rx zone due to the high volume of grains compared to the substrate material. The non-linearity of crack path caused by the increased grain boundary network would decrease the crack growth rate compared the substrate alloy; this effect would likely be minimal however, given the small grain size causing only minor crack deviations. For longer oxidation exposures, the Rx zone will increase in depth and it is therefore hypothesised that, similar to the γ′ depleted plastic zone, 5 µm exposures will have a greater benefit from this crack retardation compared to the other thermal exposures. Transmission Kikuchi Diffraction (TKD), also known as transmission Electron Backscatter Diffraction (t-EBSD) mapping was conducted to determine if the fine grain recrystallised layer was visible, the results of which are shown in Fig. 7.

The reason for the low indexing of the TKD scan is because the grains are so small that there is interaction between multiple grains through the thickness of the foil, giving overlapping Kikuchi bands, meaning there is not a clear pattern for the system to resolve. The data is however useful, as it is possible to see that there are grains in the partially γ′ depleted zone that are clearly smaller than the 4–11 µm prior grain size. It would appear that within the partially γ′ depleted zone there are a number of sub-micron grains or structures, that are smaller than the base superalloy grain structure. To support the TKD, high magnification TEM imaging was undertaken in this region, in order to more clearly display these small grains/ structures. It can be seen from Fig. 8(a) that there is a very fine grain structure in the partially γ′ recrystallised zone. Fig. 8(b) shows a SAD pattern from the circled area shown in Fig. 8(a), this area is polycrystalline with a strong texture (e.g. {011}⟨211⟩ brass texture). The formation of surface oxides will produce strain subsurface of the alloy, which promotes deformation of the subsurface via dislocation slip and/or twinning. When the deformation is large enough, it may lead to the formation of new grains with a smaller size. If those refined grains were evolved from a prior grain and not completely recrystallised, the grains would show a strong texture which is related to the prior grain.

Fatigue crack initiation from surface sites has been found to be strongly linked to surface condition, and surface initiations were the primary initiation sites for the thermal exposure specimens, as can be seen in Fig. 9. Therefore the understanding of the effect of the thermal exposures on the peened surface must be implicit.

The specimens were peened prior to their thermal exposures and it has been found for a range of superalloys that time at temperature acts to remove or partly reduce the beneficial residual stresses imparted on the alloy by shot peening [5,34–36]. The thermal exposures in this study

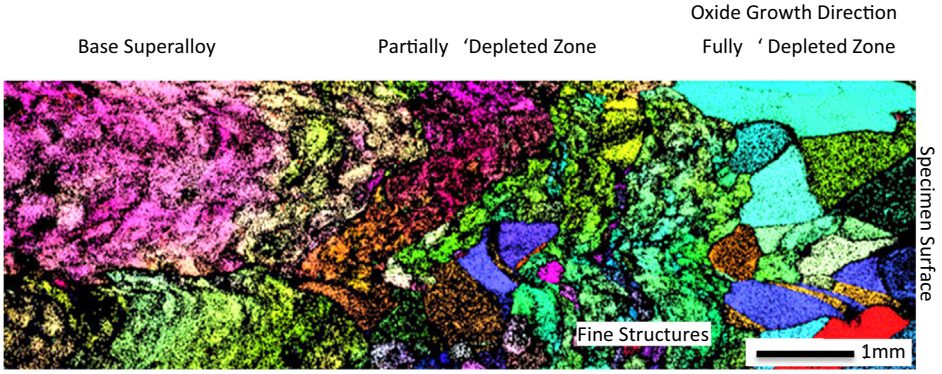

Fig. 7. TKD IPF map of the surface of the alloy with legend.

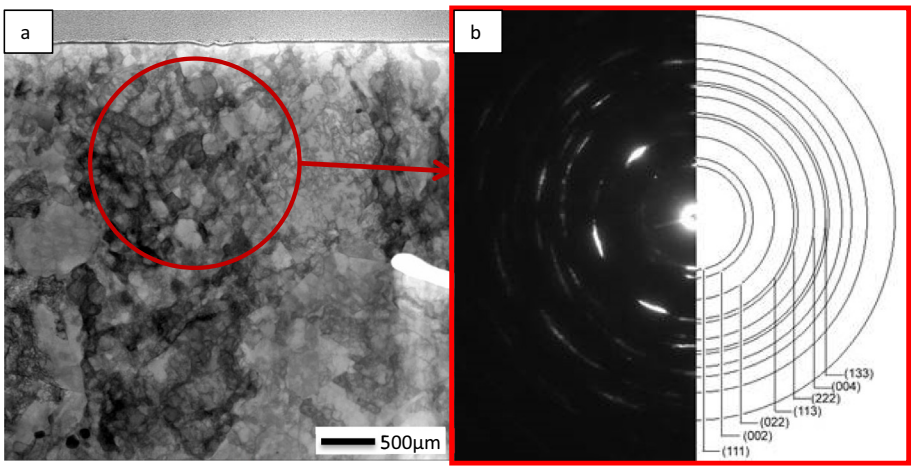

Fig. 8. (a) Bright field STEM image of recrystallisation in partially γ′ depleted zone (b) SAD pattern from the marked area.

are all longer than those found in the work performed by Khadhraoui et al. [34], Foss et al. [5] and Kim et al. [35], suggesting that the residual stress relaxation will have reached a stable point. If any beneficial residual stresses remained in the specimens the act of thermomechanical loading could reduce or remove any remainder [36–40]. However, shot peening can contribute to fatigue life in a more complex manner, even if residual stress does not have a marked effect, as a great deal of damage is being done to the shot peened surface, creating numerous potential crack initiation sites. Using a profilometer, it was hoped to improve the understanding of the effect the oxide scale growth has on the surface roughness. If the chromium oxide scale would act to 'heal' the surface this may act to reduce the crack initiation rates by decreasing the effective K_t value of the specimen surface. An example of a profilometer map that was used to calculate the S_a surface roughness value can be seen in Fig. 10.

The S_a values calculated from the Alicona profilometer data according to ISO 25178, accurate to 3 decimal places can be seen in Table 4.

As can be seen, the increased oxidation will act to reduce the surface roughness, supporting the hypothesis and the decrease in the S_a may link to the increased fatigue life of the 5 µm exposure specimens. However, the reduction in surface roughness corresponds directly to the length of the thermal exposure, suggesting that if an improvement were to occur as a result of the surface condition it would occur for all the thermal exposure conditions to some extent. It therefore appears that of all the option explored here, the coarsening of the γ′ is the most likely mechanism to have affected the fatigue lives of the 5 µm specimens. The extended heat treatment applied allows enough time for microstructural evolution, which may have affected the creep response, or overall strength of the alloy, causing the increased fatigue life.

When considering the industrial significance of the data it must be considered that service components will rarely, if ever, have geometries similar to plain specimens. As such, a number of notch fatigue tests were performed to more accurately replicate service conditions. The graph in Fig. 11 shows the S-N data from these tests. The 3 µm thermal exposure was used on these specimens as it previously showed the greatest life debit, and it was hoped this would give the greatest contrast to the AR specimens.

As can be seen, when compared to the dramatic life decrease experienced by the plain specimens due to the 3 µm exposure, the difference in life between the AR and the 3 µm exposure notched specimens for both the shallow and deeper notches are very modest. The life reduction experienced by the shallower notch was more remarkable than that of the deeper notched specimens. However, both are negligible in comparison to the large debit shown from plain fatigue testing. This suggests that the fatigue lives of the specimens at these stresses and temperature are based primarily on crack initiation rather than propagation. It is therefore suggested that in the case of the notched specimens, the notch is the cause of the initiation, and there is a more extended period of crack propagation, whereas for the heat treated plain specimens the oxide was the main initiation point and subsequent crack propagation formed only a small part of the overall specimen life, as shown by the EIS calculations. In the notched specimens, the stress raiser acts to override the effect of the extra damage imparted on the specimen by the oxide damage, making it less of a factor in the resulting crack initiation and by extension its overall fatigue life.

4. Conclusions

(1) Thermal exposures cause a dramatic drop in fatigue life compared to as received material with a 90% drop to the 1 µm exposure specimens and a further drop following the 3 µm exposure.
(2) The 5 µm exposure fatigue lives were improved compared to

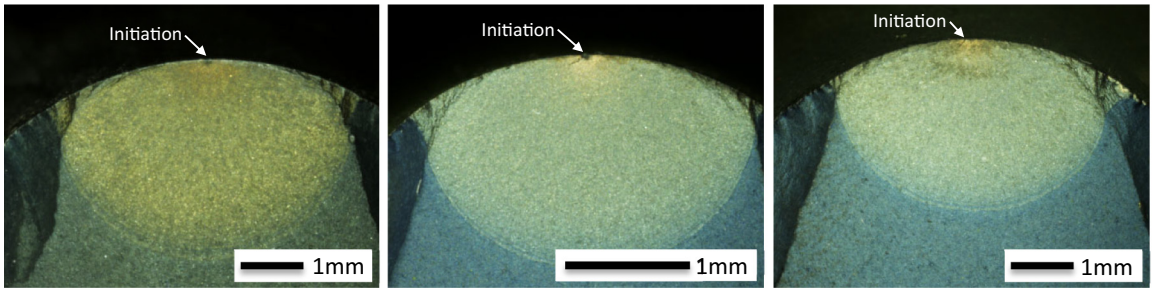

Fig. 9. Fracture surfaces of failed thermal exposure fatigue specimens with 1 µm exposure (left), 3 µm exposure (centre) and 5 µm exposure (right).

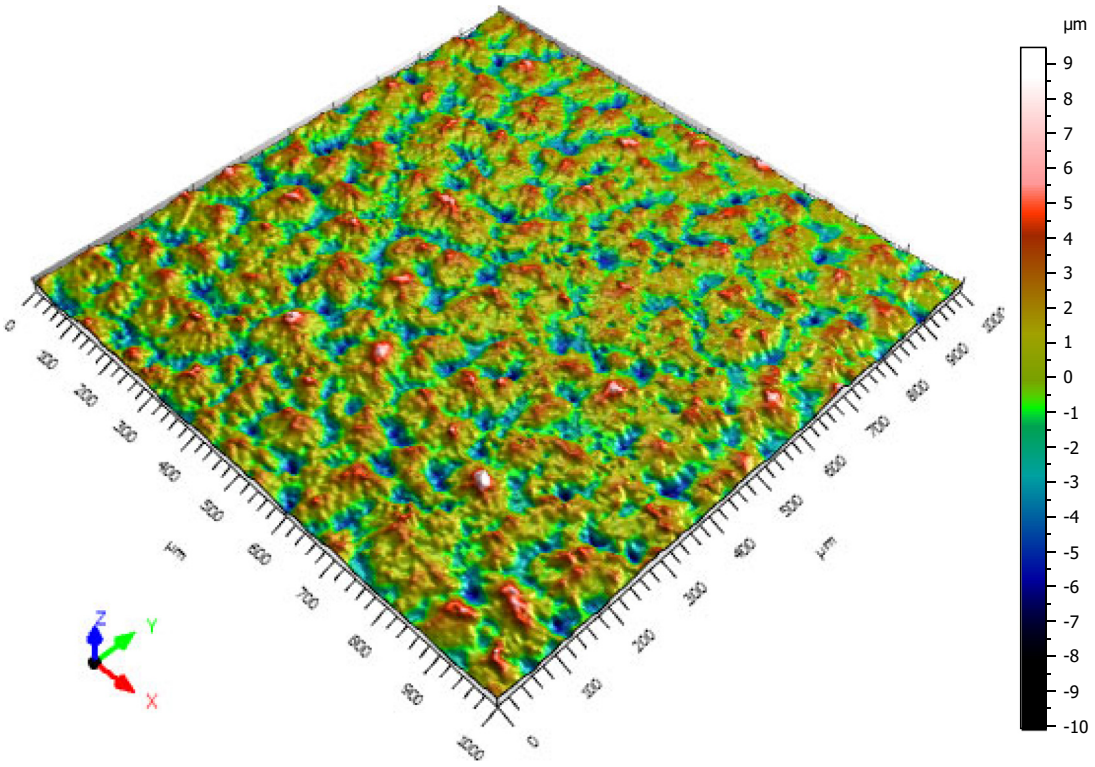

Fig. 10. Surface profile map for AR peened specimen.

those of the 3 µm exposure, with the SN curve sitting between the 1 µm exposure and 3 µm exposure curves.

a. There were no significant changes in the bulk mechanical properties as evidenced by small punch testing as a result of the different oxidising thermal exposures.
b. Tertiary γ′ coarsening may have played an role in the unexpected life improvement:
   i. Initial fatigue tests following vacuum thermal exposures showed no improvement compared to as received specimens, however other factors may contribute.
   ii. Predictive values showed a dramatic increase in the size of the tertiary γ′ as a result of the range of thermal exposures, leading to alterations in the mechanical properties of the alloy in terms of creep and potentially yield stress.
c. XPM nanoindentation showed evidence of significant differences in hardness between the oxide layer, the base material and the Rx (γ′ depleted) zone. The interaction of these zones may contribute to variations in crack initiation.
d. Recrystallised grains were found near the surface possibly leading to improved fatigue lives due to dislocation movement reduction and fatigue crack deflection mechanism.
e. The surface roughness decreases with increasing length of thermal exposure and it is hypothesised that this is due to the effect of the chromium oxide scale 'healing' the peened surface. The extent to which this would affect the crack initiation rates is unclear.

Table 4
S_a surface roughness values produced by different thermal exposures.

Thermal exposure	S_a value (µm)
As received	1.353
1 µm exposure	1.328
3 µm exposure	1.308
5 µm exposure	1.277

(3) It is likely that a combination of factors contributes to the increase in fatigue life of the 5 µm exposure specimens, including the reduction of dislocation movement rates, Rx crack deflection, interaction of different hardness zones and surface roughness reductions.
(4) For the notched fatigue specimens, the effect of oxide damage on fatigue life was considerably reduced compared to that of the plain specimens.

Declaration of competing interest

The authors declare that they have no known competing financial interests or personal relationships that could have appeared to influence the work reported in this paper.

CRediT authorship contribution statement

D.T.S. Lewis: Investigation, Writing - original draft. **R.G. Ding:** Investigation. **M.T. Whittaker:** Project administration, Supervision, Writing - review & editing. **P.M. Mignanelli:** Project administration, Supervision, Writing - review & editing. **M.C. Hardy:** Project administration, Supervision, Writing - review & editing.

Acknowledgements

The current research was funded by the EPSRC Rolls-Royce Strategic Partnership in Structural Metallic Systems for Gas Turbines (grants EP/H500383/1 and EP/H022309/1). The provision of materials and technical support from Rolls-Royce plc is gratefully acknowledged.

I would like to acknowledge the assistance provided by the Swansea University AIM Facility, which was funded in part by the EPSRC (EP/M028267/1), the European Regional Development Fund through the

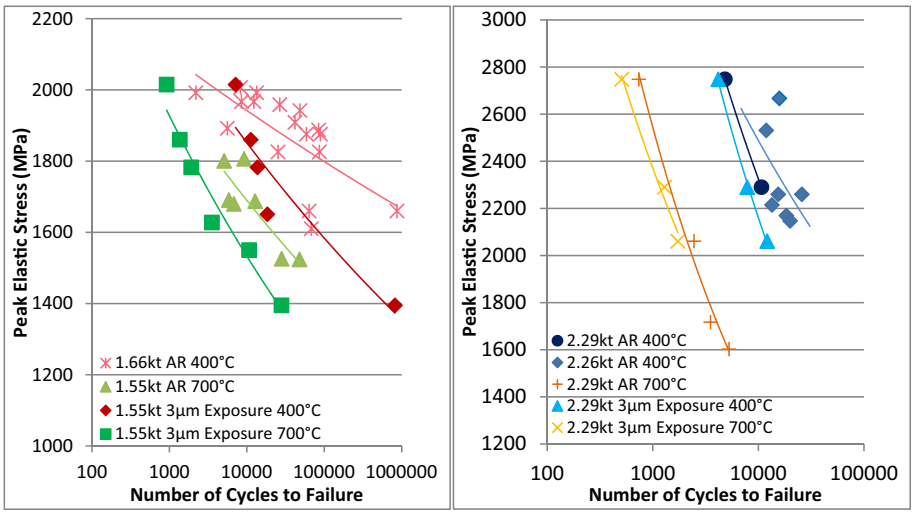

Fig. 11. Graphs showing the effect of notches on the S-N response of the alloy after exposure (a) left - showing shallower 1.55 Kt notch data and (b) right – showing deeper 2.26 Kt and 2.69 Kt notch data.

Welsh Government (80708) and the Ser Solar project via Welsh Government.

The use of equipment supplied by the Materials and Manufacturing Academy (M2A) supported through the European Social Fund is gratefully acknowledged.

We would like to acknowledge the Welsh Centre for Printing and Coating for access to their facilities and equipment in order to perform this work.

Data availability statement

The raw/processed data required to reproduce these findings cannot be shared at this time as the data also forms part of an ongoing study.

References

[1] S. Cruchley, M.P. Taylor, R. Ding, H.E. Evans, D.J. Child, M.C. Hardy, Comparison of chromia growth kinetics in a Ni-based Superalloy, with and without shot-peening, Corros. Sci. 100 (2015) 242–252.
[2] S. Cruchley, M.P. Taylor, H.Y. Li, H.E. Evans, P. Bowen, D.J. Child, M.C. Hardy, Effect of prior oxidation on high cycle fatigue performance of RR1000 and role of oxidation in fatigue crack initiation, Mater. High Temp. 32 (1–2) (2015).
[3] S. Cruchley, H.Y. Li, H.E. Evans, P. Bowen, D.J. Child, M.C. Hardy, The role of oxidation damage in fatigue crack initiation of an advanced Ni-based superalloy, Int. J. Fatigue 81 (2015) 265–274.
[4] S. Cruchley, H.E. Evans, M.P. Taylor, M.C. Hardy, S. Stekovic, Chromia layer growth on a Ni-based superalloy: sub-parabolic kinetics and the role of titanium, Corros. Sci. 75 (2013) 58–66.
[5] B.J. Foss, S. Gray, M.C. Hardy, S. Stekovic, D.S. McPhail, B.A. Shollock, Analysis of shot-peening and residual stress relaxation in the nickel-based superalloy RR1000, Acta Mater. 61 (2013) 2548–2559.
[6] H.S. Kitaguchi, H.Y. Li, H.E. Evans, R.G. Ding, I.P. Jones, G. Baxter, P. Bowen, Oxidation ahead of a crack tip in an advanced Ni-based superalloy, Acta Mater. 61 (2013) 1968–1981.
[7] C.K. Sudbrack, S.L. Draper, T.T. Gorman, J. Telesman, T.P. Gabb, D.R. Hull, Oxidation and the effects of high temperature exposures on notched fatigue life of an advanced powder metallurgy disk superalloy, Superalloys 2012 2012, pp. 863–872.
[8] D.W. Hunt, The Stability and Mechanical Properties of a Nickel-Base Turbine Disc Alloy, University of Oxford, 2001.
[9] R.C. Reed, The Superalloys, fundamentals and applications, The Superalloys, 2006 , (p. various).
[10] A.J. Manning, D. Knowles, C.J. Small, Nickel Based Superalloy, US 7,208,116 B2 2007.
[11] T.P. Gabb, C.K. Sudbrack, S.L. Draper, R.A. MacKay, J. Telesman, Effects of long term exposures on fatigue of PM disk superalloys, Mater. Perform. Charact 3 (2) (2013).
[12] A. Karabela, L.G. Zhao, J. Tong, N.J. Simms, J.R. Nicholls, M.C. Hardy, Effects of cyclic stress and temperature on oxidation damage of a nickel-based superalloy, Mater. Sci. Eng. A 528 (19–20) (2011) 6194–6202.
[13] J.H. O'Hanlon, M.C. Hardy, D.J. Child, B. Foss, P.J. Withers, M.R. Bache, The effect of minimum dwell cycles on the environmental and fatigue response of RR1000, MATEC Web of Conferences, 14, , 2014.
[14] A. Karabela, L.G. Zhao, B. Lin, J. Tong, M.C. Hardy, Oxygen diffusion and crack growth for a nickel-based superalloy under fatigue-oxidation conditions, Mater. Sci. Eng. A 567 (2013) 46–57.
[15] M.R. Bache, J.P. Jones, G.L. Drew, M.C. Hardy, N. Fox, Environment and time dependent effects on the fatigue response of an advanced nickel based superalloy, Int. J. Fatigue 31 (11–12) (2009) 1719–1723.
[16] R.J. Mitchell, J.A. Lemsky, R. Ramanathan, H.Y. Li, K.M. Perkins, L.D. Connor, Process development and microstructure and mechanical property evaluation of a dual microstructure heat treated advanced nickel disc alloy, Superalloys 2008 2008, pp. 347–356.
[17] CEN Workshop Agreement, CWA 15627: Small Punch Test Method for Metallic Materials, Brussels, Belgium, 2007.
[18] F. Schulz, H.Y. Li, H. Kitaguchi, D. Child, S. Williams, P. Bowen, Influence of tertiary gamma prime (γ′) size evolution on dwell fatigue crack growth behavior in CG RR1000, Metall. Mater. Trans. A Phys. Metall. Mater. Sci. 49 (2018) 3874–3884.
[19] T.P. Gabb, J. Gayda, D.F. Johnson, R.A. MacKay, R.B. Rogers, C.K. Sudbrack, A. Garg, I.E. Locci, S.L. Semiatin, E. Kang, Comparison of γ-γ' Phase Coarsening Responses of Three Powder Metal Disk Superalloys, no. February 2016 44.
[20] T.P. Gabb, J. Gayda, J. Telesman, A. Garg, in: R. Reed (Ed.), The effects of heat treatment and microstructure variations on disk Superalloy properties at high temperature, Superalloys 2008: 11th International Symposium on Superalloys, TMS 2008, pp. 807–816.
[21] J. Telesman, T.P. Gabb, A. Garg, P. Bonacuse, J. Gayda, Effect of microstructure on time dependent fatigue crack growth behavior in a P/M turbine disk alloy, Proceedings of the International Symposium on Superalloys (2008).
[22] M.C. Chaturvedi, Y. Han, Effect of particle size on the creep rate of superalloy Inconel 718, Mater. Sci. Eng. 89 (1987) L7–L10.
[23] P.L. Threadgill, B.B. Wilshire, The effect of particle size and spacing on creep of two-phase copper–cobalt alloys, Met. Sci. 8 (1974) 117–124.
[24] W. Elber, Fatigue crack closure under cyclic tension, Eng. Fract. Mech. 2 (1) (1970) 37–44.
[25] W. Elber, The significance of fatigue crack closure, Damage Tolerance in Aircraft Structures, ASTM International 1971, pp. 230–242.
[26] C.S. Lee, C.G. Park, Y.W. Chang, Precise determination of fatigue crack closure in Al alloys, Mater. Sci. Eng. A 216 (1–2) (1996) 131–138Oct.
[27] E.D. Hintsala, U. Hangen, D.D. Stauffer, High-throughput nanoindentation for statistical and spatial property determination, JOM 70 (4) (2018) 494–503.
[28] B.J. Foss, M.C. Hardy, D.J. Child, D.S. McPhail, B.A. Shollock, Oxidation of a commercial nickel-based superalloy under static loading, JOM 66 (12) (2014).
[29] K.F. Amouzouvi, L.J. Clegg, R.C. Styles, J.E. Winegar, Effect of shot peening and post-peening heat treatments on the microstructure, the residual stresses and hardness, corrosion and deuterium uptake resistance of Zr-2.5Nb pressure tube material, Trans. Eng. Sci 2 (1993) 145–154.
[30] Z. Li, Q. Xu, B. Liu, Microstructure simulation on recrystallization of an as-cast nickel based single crystal superalloy, Comput. Mater. Sci. 107 (2015) 122–133.
[31] N. Sheng, K. Horke, A. Meyer, M.R. Gotterbarm, R. Rettig, R.F. Singer, Surface recrystallization and its effect on oxidation of superalloy C263, Corros. Sci. 128 (April) (2017) 186–197.
[32] S. Suresh, Fatigue of Materials, 2nd ed. Cambridge University Press, Cambridge, 1998.
[33] S. Suresh, Crack deflection: implications for the growth of long and short fatigue cracks, Metall. Trans. A. 14 (1983) 2375–2385.
[34] M. Khadhraoui, W. Cao, L. Castex, J.Y. Guédou, Experimental investigations and modelling of relaxation behaviour of shot peening residual stresses at high temperature for nickel base superalloys, Mater. Sci. Technol. 13 (1997) 360–367.
[35] S.B. Kim, A. Evans, J. Shackleton, G. Bruno, M. Preuss, P.J. Withers, Stress relaxation of shot-peened UDIMET 720Li under solely elevated-temperature exposure and under

isothermal fatigue, Metall. Mater. Trans. A Phys. Metall. Mater. Sci. 36A (2005) 2005–2041.
[36] W. Cao, M. Khadhraoui, B. Brenier, J.Y. Guedou, L. Castex, Thermomechanical relaxation of residual stress in shot peened nickel base superalloy, Mater. Sci. Technol. 10 (1994).
[37] A. Evans, S.B. Kim, J. Shackleton, G. Bruno, M. Preuss, P.J. Withers, Relaxation of residual stress in shot peened Udimet 720Li under high temperature isothermal fatigue, Int. J. Fatigue 27 (10–12) (2005) 1530–1534.
[38] R. John, D.J. Buchanan, M.J. Caton, S.K. Jha, Stability of shot peen residual stresses in IN100 subjected to creep and fatigue loading, Procedia Engineering 2 (1) (2010) 1887–1893.
[39] D.J. Buchanan, R. John, Relaxation of shot-peened residual stresses under creep loading, Scr. Mater. 59 (3) (2008) 286–289.
[40] D.J. Buchanan, R. John, R.A. Brockman, Relaxation of shot-peened residual stresses under creep loading, J. Eng. Mater. Technol. Trans. ASME 131 (3) (2009) 0310081–03100810.